Soft Matter

PAPER

View Article Online
View Journal | View Issue

Cite this: *Soft Matter*, 2017, 13, 2099

Particle–wall tribology of slippery hydrogel particle suspensions

Heather M. Shewan,*[a] Jason R. Stokes[a] and Michel Cloitre[b]

Received 2nd August 2016,
Accepted 3rd February 2017

DOI: 10.1039/c6sm01775d

rsc.li/soft-matter-journal

Slip is an important phenomenon that occurs during the flow of yield stress fluids like soft materials and pastes. Densely packed suspensions of hydrogel microparticles are used to show that slip is governed by the tribological interactions occurring between the samples and shearing surfaces. Both attractive/repulsive interactions between the dispersed particles and surface, as well as the viscoelasticity of the suspension, are found to play key roles in slip occurring within rheometric flows. We specifically discover that for two completely different sets of microgels, the sliding stress at which slip occurs scales with both the modulus of the particles and the bulk suspension modulus. This suggests that hysteresis losses within the viscoelastic particles contribute to friction forces and thus slip at the particle–surface tribo-contact. It is also found that slip during large amplitude oscillatory shear and steady shear flows share the same generic features.

1. Introduction

A key feature of yield stress materials is their propensity to slip when sheared along solid surfaces.[1,2] In rheometry, slip is generally considered an inconvenience that must be controlled or eliminated to measure the rheological properties of materials without geometric artefacts.[3] In many real situations, it is precisely the ability of soft materials to slip that allows them to move readily and efficiently. Slip is essential within many natural systems, including transport of solid foods through the oral, digestion and waste pathways,[4] the movement of blood cells through narrow arteries,[5] the adhesive locomotion of gastropods,[6] or the nutrient delivery by cytoplasmic streaming in plant cells.[7] The importance of the phenomena of wall slip in applications is also seen in the transport of many complex suspensions, such as oil emulsions, foods, pharmaceuticals, sewage treatment and soils.[8–11] During processing of composites or nanocomposites in extruders and slit dies, it is crucial to account for slip phenomena which cannot be avoided in general.[12–14] The occurrence of slip has also important consequences on the development of flow instabilities during the extrusion of highly filled polymeric suspensions,[15,16] the spreading of yield stress fluids,[17,18] and the establishment of steady conditions during start up flows or cessation flows of yield stress materials.[19,20] Hence the occurrence of slip for complex materials must be considered as an important and intrinsic feature of its flow and deformation behaviour.

Mooney introduced a method to analyze slip and measure slip velocities in capillary and rotational rheometry; these rely on multiple measurements performed with the same capillary length over diameter ratios but different diameters or different parallel plate gap sizes, respectively.[21] The only hypothesis for any geometry is that the slip velocity depends only on the wall shear stress and not on other quantities like the normal stresses. The method was later revisited and simplified by Yoshimura and Prud'homme.[3] It has been used to characterize wall slip velocities in various materials.[22–25] The method is appealing from a macroscopic point of view but it is time consuming and subject to practical limitations like the difficulty to vary the gap size over a wide range of values. Moreover it does not provide much information about the microscopic origin of slip.

Slip properties are generally characterized by a slip boundary condition which relates the slip velocity to the wall shear stress. An important and open question consists in connecting the form of the slip equation to the microscopic phenomena at the origin of slip. The generic reason for slip of particle suspensions is depletion of the dispersed phase away from the surface, leading to a thin film of solvent between the surface and the dispersed phase.[26] Because of the presence of shear within the interfacial low-viscosity film, slip is said to be apparent rather than true, as occurs in sliding a solid object over a surface.[1,27] The physical origin of slip layers in concentrated suspensions is apparently not universal and depends on the microstructure of the suspensions.

In concentrated Brownian or non-Brownian rigid particle suspensions, different mechanisms have been proposed to cause particle depletion: steric depletion,[22,23,28–30] particle migration driven by gradients in shear rate or a non equilibrium particle

[a] School of Chemical Engineering, The University of Queensland, Building 74, Brisbane, Queensland, Australia. E-mail: h.shewan@uq.edu.au
[b] Soft Matter and Chemistry, CNRS, ESPCI Paris, PSL Research University, 10 rue Vauquelin, 75005 Paris, France

pressure,[31] repulsive wall–particle forces.[32] It is also dependent on the particle wall interactions, as shown by particle tracking microvelocimetry.[29]

Slip in concentrated soft particle suspensions, such as colloidal pastes or emulsions, has attracted a lot of attention in the recent years.[33–42] These materials have a close-packed amorphous structure and flow past one another appreciably only when a large enough stress is applied, greater than the so-called yield stress. For steady shear flows, Meeker *et al.* proposed a model where the particle deformation is coupled to the flow through the pressure field so that the flat contacts existing between the particles and the bounding surfaces are deformed asymmetrically.[34,35] The asymmetry breaks the reversibility of the Stokes equation and generates a lift force pushing the particles away from the moving surfaces. The balance between the lift force and the bulk osmotic pressure of the suspension sets the thickness of the lubricated layer. This model, which relies on elastohydrodynamic lubrication (EHL) predicts a slip law where the slip velocity is a quadratic function of the shear stress. Later on, Seth *et al.* incorporated the action of attractive or repulsive interactions between the slipping particle and the wall.[36] They proposed to relate the existence of a slip yield stress to the short range surface forces between the particles and the wall. In addition to the EHL slip mechanism, Seth *et al.* also predicted the existence of a second slip regime driven by simple hydrodynamic lubrication (HL) when the lubricating film thickness exceeds the range of surface forces. Provided that the suspending fluid is Newtonian, the stress–velocity relationship is linear and there is no slip yield stress.[23,36,40,42] This description has been applied with some success to concentrated suspensions of colloidal microgels subjected to steady shear flow.[36,37,40,42] However important questions remain open concerning the applicability of the model to a wide range of soft materials subject to various types of mechanical solicitations like unsteady flows,[43] and the exact relation between particle scale properties and slip.

The objective of this work is to elucidate the microscopic origin of slip in a new class of non-colloidal soft microparticles and to relate particle properties to macroscopic behaviour in terms of EHL slip. The particles have a well-defined modulus allowing us to relate the interactions between the soft particles and the substrate to the onset of slip and to the characteristic slip velocity. These hydrogel particles have previously been shown to be a simple model system for a variety of yielding soft matter systems,[10,44–46] as well as being useful for rheology control and encapsulation.[47,48] We analyze slip both in steady shear flows and Large Amplitude Oscillatory Shear (LAOS) which represents a model situation of unsteady solicitation where the material is periodically returned to the same state of deformation without necessarily having time to relax. We show that the slip behaviour in both types of flow can be mapped onto one another to allow us to define the deformation ranges where slip is significant. Using two different wall surfaces, which are hydrophilic and hydrophobic respectively, we find that the slip properties of agarose microparticles are controlled by EHL lubrication. In addition, we show that for two completely different sets of microgels, the slip stress at which slip occurs scales with both the modulus of the particles and the bulk suspension modulus. This suggests that the viscoelastic particles contribute to friction forces and thus slip at the particle–surface. The paper is organized as follows. In Section 2, we describe the manufacture of the agarose microparticles and the rheometric techniques implemented to investigate their bulk and surface properties. In Section 3, we present the experimental results obtained in oscillatory and steady shear flows. In Section 4, we analyse the microscopic origin of slip and the consequences on the particle–wall tribology of these materials.

2. Materials and methods

2.1 Agarose microparticle manufacture

Agarose microparticles were manufactured following an emulsion-gelation route similar to that used by Adams *et al.*[46] Agarose solutions were prepared by adding agarose at a concentration of 1.5 weight percent to water purified by reverse osmosis, resistivity of 18.2 MΩ cm, containing 0.02% sodium azide and heating to 95 °C for 30 minutes while stirring. The agarose solution was allowed to stand without stirring for 5 minutes to allow air bubbles to escape. A water-in-oil emulsion was formed by adding the agarose to sunflower oil at weight ratio of 30 : 60. To promote formation and stability of the emulsion during the process, 1 weight percent polyglycerol polyricinoleate (Admul WOL) at 80 °C was used. The mixture was homogenised using an IKA Ultra Turrax at 80 °C and 12 000 rpm for 12 minutes to allow an equilibrium particle size to develop. The emulsion was quenched by placing in an iced water bath to gel the aqueous phase while stirring at 300 rpm for 2 hours to prevent aggregation and coalescence. The spherical particles produced were separated from the oil phase by five cycles of centrifugation (8000 rpm for 40 minutes) washing with ethanol followed by RO water, and filtered through a 20 μm mesh using a Buchner filter and flask under vacuum to remove large particles. Suspensions were made to known wet weight percentages from 70% to 90% by redispersing the particles in RO water.

The properties of individual particles were analysed at low dilution using different techniques. Fig. 1a presents an optical microscope photograph of a dilute suspension observed at high magnification using the contrast phase technique (lens: PL APO 63 × 1.32 oil). We clearly distinguish small spherical particles. Fig. 1b shows the particle diameter distribution which was measured with a Malvern Mastersizer. From these data we compute the quantities reported in Table 1: the average particle diameter ($d_{0.5}$), the volume weighted mean ($d_{4.3}$), the surface weighted mean ($d_{3.2}$), and the standard deviation for a log normal distribution (std = $\ln(d_{4.3}/d_{3.2})$).

In the following, it is convenient to characterize the microgel suspensions at finite concentration by the weight fraction C. The weight fraction C and the actual volume fraction ϕ are related through an equation of the form: $\phi = K(C)C$, where the coefficient K is the specific volume. At low concentrations, K can be considered as constant and can be determined following a well-established procedure.[49,50] At high concentration, some

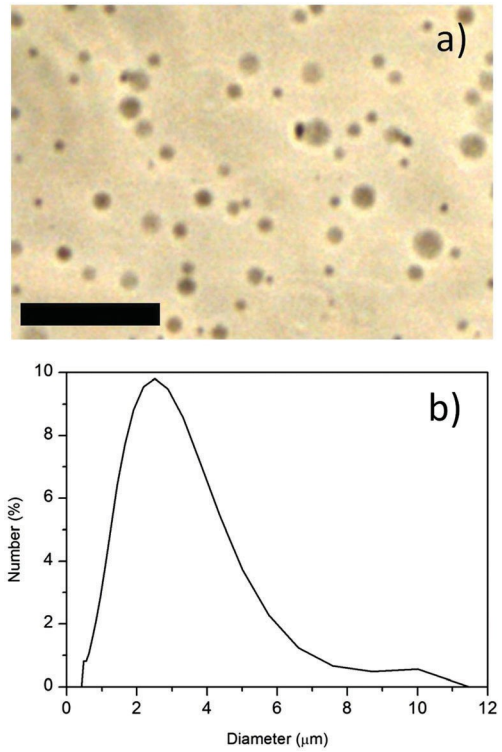

Fig. 1 (a) Optical microscopy observation of dilute agarose suspension; scale bar is 10 microns. (b) Volume weighted size distribution of agarose microgels.

Table 1 Characterization of agarose microgels; $d_{0.5}$: average particle diameter; $d_{4.3}$: volume weighted mean diameter; $d_{3.2}$: surface weighted mean diameter; std = $\ln(d_{4.3}/d_{3.2})$: standard deviation for log normal distribution; K: specific volume; C_{rcp}: close-packing weight fraction from particle size distribution; G_p: shear modulus

$d_{0.5}$ (mm)	$d_{4.3}$ (mm)	$d_{3.2}$ (mm)	std	K (ml g^{-1})	C_{rcp} (g g^{-1})	G_p (kPa)
2.2	2.4	1.8	0.29	73.0	0.71	64

deswelling can occur and affect the value of K determined at infinite dilution, as it was observed in other soft particle suspensions.[49,51] The random close packing volume fraction is determined from the particle size distribution, independent of the rheology, using the method of Farr and Groot[52] as described in Shewan and Stokes.[53]

2.2 Rheological measurements

Rheological measurements were carried out on a rotational rheometer MCR 501 from Anton Paar. In all studies of slip behaviour, it is necessary to have a benchmark non-slip case using a roughened surface with roughness of at least the same order as the particle size. We investigated a range of sandpaper and sandblasted surfaces and determined that both the sand-blasted surface provided by Anton Paar on their cone and plate geometry with roughness of the order of 20 mm and wet/dry 120 grit sandpaper were sufficient to prevent slip. A 25 mm cone sandblasted to a roughness of about 20 mm is used in combination with a bottom plate that was either: roughened; made hydrophobic by covering with Scotch tape, a polymer film derived from cellulose acetate (contact angle with water: 80 degrees); or made hydrophilic by attaching a silicon wafer (contact angle with water: 13±3 degrees). These surfaces were prepared as described by Seth *et al.*[36] To ensure that all suspensions had the same shear history and to eliminate any possible influence of evaporation a new loading from the same sample was used for each measurement. We then conducted two types of rheological tests, oscillatory and steady shear experiments, for both rough and smooth bottom plates.

Oscillatory frequency sweeps were used to measure the variations of the storage modulus G' and loss modulus G'' as functions of the angular frequency $\omega(10^{-2} \le \omega \le 10^{2}$ rad s$^{-1})$ at small strain amplitudes in the linear viscoelastic regime ($\gamma = 5 \times 10^{-3}$). The storage and loss moduli showed the characteristic variations exhibited by other soft glassy materials, *i.e.* a nearly constant plateau in $G'(\omega)$ and a much lower $G''(\omega)$ with a small minimum around a frequency ω_m. We defined the plateau modulus of the suspension, G_0, as the value of $G'(\omega)$ at ω_m. Oscillatory strain sweep experiments were performed by applying a periodic strain at a fixed angular frequency $\omega = 1$ rad s^{-1} in order to obtain the variations of σ, G' and G'' with the strain amplitude γ ($10^{-3} \le \gamma \le 10$) and to characterize the yielding properties. We checked that the results are insensitive to the angular frequency within the experimental accuracy. Finally, oscillatory time sweeps at $\gamma = 6 \times 10^{-3}$ and $\omega = 1$ rad s^{-1} were performed at the beginning and end of each sequence of measurements to verify that rheological properties of the sample had not been altered.

Steady shear experiments were performed as follows: the suspension was first sheared from 0.05 s^{-1} to 500 s^{-1} in 21 steps using 30 seconds per step, then sheared from 500 s^{-1} down to 0.05 s^{-1} in 21 steps using again 30 seconds per step. $\sigma(\dot{\gamma})$ data for slip and flow analysis were taken from the final decreasing shear rate sweep. Measurements for the second and subsequent sequence of solicitations were repeatable showing that the materials are at steady state.

2.3 Determination of the particle modulus

The particle modulus, G_P, was assumed to be equivalent to the modulus of a bulk agarose gel and was determined as follows. The modulus of bulk gel disks was measured using parallel plate geometry. Agarose solutions were prepared at 80 °C and poured onto the non-slip (sandpaper) plate surface pre-heated to 80 °C. The plates were brought together to the required gap, the excess solution carefully trimmed and the temperature set point reduced to 25 °C to induce gelation. The gels were allowed5 minutes equilibration time after the temperature set point was reached. An amplitude sweep was run to determine the linear viscoelastic region at high and low frequency followed by a frequency sweep across this range. The particle modulus determined by this method is $G_P = 64$ kPa (Table 1).

3. Results

3.1 Yielding behaviour of concentrated agarose suspensions

At low concentration, agarose microparticle suspensions have a purely viscous behaviour qualitatively similar to that of hard

sphere suspensions except at large concentrations where they can undergo some de-swelling as usually observed in polymer microgels.[50] Above a concentration we assign to be the close-packing concentration, which was determined independently from the particle size distribution,[50,53] the suspensions become solid-like at rest but yield when a sufficiently large stress is applied.

We conducted systematic strain sweep experiments in the jammed regime using smooth and rough bottom plates. The variations of the storage and loss moduli, G' and G'', and of the stress amplitude, σ, with the strain amplitude, γ, for an agarose particle suspension at $C = 0.85$ g g^{-1} are represented in Fig. 2. The results for the other concentrations and angular frequencies are qualitatively the same.

When both the top and bottom plates are rough (*i.e.* in the absence of slip), G', G'', and σ have the characteristic shapes found in other soft particle jammed suspensions like polyelectrolyte microgels,[54] star polymer solutions,[55] and emulsions.[56] At small strain amplitudes, the stress is linear with the strain, indicating that the rheological response is in the linear regime. The suspension exhibits solid-like behaviour with $G' > G''$; both moduli are independent of the strain amplitude. At large amplitudes (LAOS), G' decreases whereas G'' goes through a maximum before declining and crossing the storage modulus: the onset of non-linearity is associated with yielding. For particle suspensions with repulsive interactions the weak overshoot has been attributed to localized particle motions that lead to increased dissipation.[54]

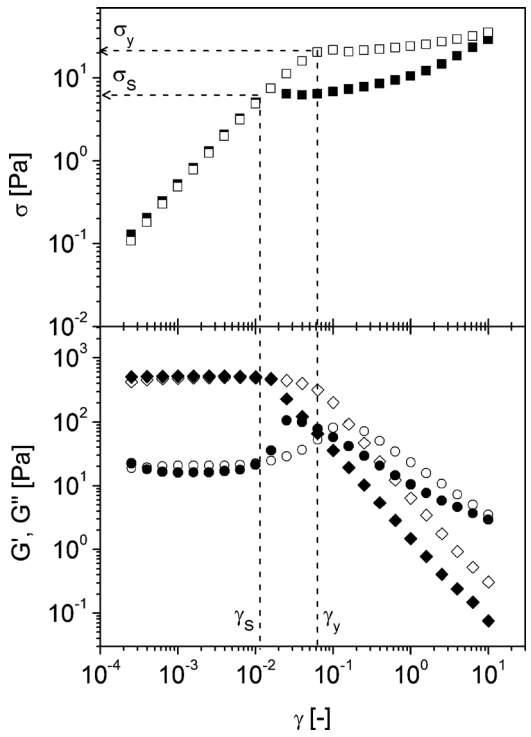

Fig. 2 Variations of stress (top; ▾, &), storage (bottom; ■; ●) and loss modulus (bottom; ◆, ◇) against maximum strain for a agarose microgel suspension at a concentration of 0.85 g g^{-1} for a rough (open symbols) and smooth silicon (full symbols) bottom plate. The angular frequency is $\omega = 1$ rad s^{-1}.

Table 2 Values of the material properties determined from small amplitude oscillatory shear (G_0: plateau storage modulus, σ_y: yield stress; γ_y: yield strain), and steady shear (σ_y: yield stress; γ_y: yield strain; k: consistency; n: shear thinning exponent)

		σ_y (Pa)	γ_y (—)	σ_y (Pa)	γ_y (—)		
C (g g^{-1})	G_0 (Pa)	LAOS		Flow		k (Pa s^n)	n
0.70	68	3.6	0.050	3.5	0.05	0.68	0.61
0.75	125	5.9	0.55	5.6	0.05	1.08	0.57
0.80	225	9.1	0.055	8.3	0.04	1.91	0.51
0.85	518	21.7	0.06	19	0.04	4.94	0.43
0.90	620	30	0.055	27	0.04	6.7	0.39

At even larger amplitudes, both moduli decrease as power laws as already observed in many soft glassy materials. The intersection between the low strain linear variation of the stress and the high strain variation is relatively abrupt and marks the onset of yielding. It provides a quantitative determination of the yield strain and stress as depicted in Fig. 2. The values of G_0, σ_y, γ_y measured for the five concentrations studied in this manuscript are reported in Table 2. The yield stress σ_y, increases with the volume fraction and is proportional to the elastic modulus G_0 through $\sigma_y = G_0\gamma_y$ where γ_y is defined as the yield strain. γ_y takes values of a few percent in agreement with previous determinations for similar soft materials.[51,57]

When the bottom plate is smooth, *i.e.* when slip occurs, the apparent response of the suspension during a strain sweep test is drastically modified. At low strain amplitudes the variations of G', G'', and σ are nearly superimposed to the data measured with the rough plate, indicating that slip is absent and the moduli are not affected. Above a strain γ_s corresponding to a stress σ_s, the moduli and the stress begin to deviate from their values measured in the absence of slip. Interestingly the variations of G', G'', and σ are reminiscent of those observed during yielding: the apparent shear modulus begins to decline, the loss modulus increases and reaches a maximum before decreasing. However, the values of these quantities are significantly smaller than in absence of slip, the maximum of the overshot occurs at a strain smaller than γ_y as well as the strain where G'' becomes larger than G'. This apparent yielding behaviour must not be confused with the true yield point corresponding to the onset of bulk flow. It signals the point where the material begins to slip. At strain amplitude larger than the bulk yield stress σ_y, the stress values in the absence and in the presence of slip becomes equal suggesting that the effect of slip becomes negligible once the material has yielded. The values of the slip yield stress σ_s obtained from LAOS experiments for the five concentrations studied are reported in Table 3.

3.2 Flow and slip of concentrated agarose suspensions

Fig. 3 shows the flow curve of a concentrated suspension (filled symbols) at a volume fraction above close-packing ($C = 0.85$ g g^{-1}), when slip is obviated by the use of rough shearing surfaces. The flow curves have the characteristic shape expected for yield

Table 3 Slip parameters for the five suspensions considered in this study

	σ_s (Pa)	σ_s (Pa)		V^* (mm s^{-1})	V^* (mm s^{-1})	
C (g g^{-1})	LAOS	Flow	$\dot{\gamma}^*$ (s^{-1})	$= \dot{\gamma}^* h$	Eqn (2)	m
0.70	2.0	1.75	1.5	0.73	1.03	0.56
0.75	2.5	2.5	1.8	0.87	1.17	0.56
0.80	5.2	4.9	2.1	1.05	1.18	0.73
0.85	6.5	6.9	4.1	2.05	2.03	0.65
0.90	6.9	6.6	10	4.95	3.19	0.60

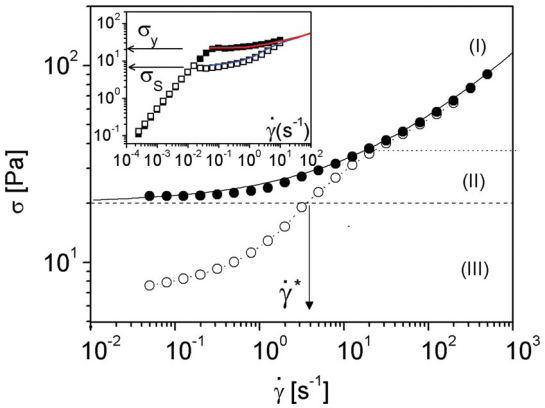

Fig. 3 Shear stress against shear rate for suspensions at C = 0.85 g g^{-1} on rough (K) and smooth silicon (J) surfaces. The vertical line indicates the critical shear rate $\dot{\gamma}^*$ below which full slip occurs. The solid line represents the fit of the data to the Herschel–Bulkley equation. The different slip regimes are limited by the dashed and the dotted lines. The inset compares the stress measured in oscillatory (◡, &) and steady shear (red line; blue line) measurements. Data for the smooth silicon surface (◡; blue line) and the rough surface (&; red line) are compared.

stress materials, *i.e.* a constant stress plateau at low shear rates (in double logarithmic coordinates) and a power law variation at high shear rates. It is well described by the Herschel–Bulkley equation of the form: $\sigma(\dot{\gamma}) = \sigma_y + k\dot{\gamma}^n$ where σ_y is the yield stress, k is the consistency parameter, and n is the shear thinning exponent. The values of these different parameters are reported in Table 2 for C = 0.70 to 0.90 g g^{-1}. The values of the yield stress and yield strain are in good agreement with the previous determination using the strain sweep amplitude technique. The value of the shear thinning exponent n varies around 0.5, which is the value expected for suspensions of a thermal soft particle suspensions; the consistency parameter k increases with G_0.[58]

The flow curves are completely modified when a smooth plate instead of a rough plate is used at the bottom, stationary surface. This is shown in Fig. 3 where we compare the flow curves measured with a silicon wafer (open symbols) and a roughened steel bottom plate (full symbols). The surface characteristics mainly affect the low shear rate regime below 10 s^{-1} where we measure significantly lower shear stresses for the silicon wafer. Again these important deviations from the flow curve measured with rough surfaces prevent us from determining the bulk yield stress reliably. This behaviour is the signature of wall slip at smooth surfaces. The apparent flow curves then characterize the lubrication properties of the suspensions at the smooth surfaces rather than their bulk rheological behaviour. The importance of wall slip is generally sensitive to the nature of the shearing surfaces through the existence of specific short range forces. Here, in contrast with previous experiments on polyelectrolyte microgels, the chemical nature of the smooth surface has little importance and a similar level of slip is evident on the hydrophilic (silicon) and hydrophobic (polymeric) surface, as shown by Shewan,[59] indicating that agarose microparticles develop similar interactions with both types of surfaces.

It is interesting to replot the stress variations measured in the LAOS experiments *versus* the shear rate and to compare the resulting flow curve to that measured in steady flow experiments. The inset in Fig. 3 shows that both sets of data agree perfectly again, in particular in the range of strain/stress where slip is dominant, confirming that slip in LAOS and steady flows share the same generic features.

4. Discussion

4.1 Analysis of slip

In Fig. 3, the apparent flow curves measured in the presence of slip reveal three different dynamical regimes. In regime I, the flow curves for the smooth and rough surfaces nearly coincide. In regime II, there begins to be a significant difference between the two sets of data and the discrepancy between them increases as the apparent shear rate is decreased. Regime III corresponds to stress values below the bulk yield stress where no macroscopic motion is expected. As the apparent shear rate decreases, the measured stress also decreases but finally extrapolates to a finite value at very low apparent shear rate. The behaviour found in Fig. 3 nicely matches previous observations for polyelectrolyte microgels and microgels.[33–35] Combining conventional rheological measurements with velocimetry, it has been shown that regime III corresponds to a pure slip regime where the material slips as a solid body on the smooth surface. Regime II is a mixed regime characterized by a combination of wall slip and bulk flow. The latter becomes dominant in regime I where slip still exists but with a negligible impact on the apparent flow curve.

4.2 Determination of slip velocity

In the following we focus on the behaviour of agarose particle suspensions in regime III. The onset of pure slip can be characterized by the value of the apparent shear rate $\dot{\gamma}^*$ where the apparent stress is equal to the bulk yield stress σ_y measured from the bulk rheology in the absence of slip. Since all the motion then comes from the slipping of the paste, $\dot{\gamma}^*$ is related to the slip velocity V^* at the onset of total slip through: $V^* = \dot{\gamma}^* h$ where h is the value of the gap at the edge of the cone (0.485 mm). The experimental values of $\dot{\gamma}^*$ and V^* for the five concentrations investigated are reported in Table 3. Below $\dot{\gamma}^*$ the paste undergoes pure slip and hence the apparent stress–shear rate relationship can be used to extract the variations of the slip velocity with the stress.

4.3 Interpretation in terms of EHL slip

The variations of the reduced slip velocities V/V^* with the shear stress are plotted in Fig. 4. The slip velocity vanishes at a stress σ_s, termed the slip yield stress which we identify as the stress below which the material sticks to the surface, therefore suppressing wall slip. σ_s is finite and of the order of a few Pascals, and increases with the volume fraction. To characterize the variations of the slip velocity in the domain $\sigma_s < \sigma < \sigma_y$, we fit the experimental data to the analytical expression:[35]

$$\frac{V}{V^*} = \left(\frac{\sigma - \sigma_s}{\sigma_y - \sigma_s}\right)^{1/m} \quad (1)$$

σ_y and V^* are known independently from the bulk rheological measurements (see Tables 2 and 3) whereas σ_s and m are two fitting parameters. The values of m and σ_y are also reported in Table 3. The exponent m is much lower than 1 and in most cases takes values between 0.5 and 0.6. This value indicates that slip in concentrated suspensions of agarose particles is driven by elastohydrodynamic lubrication.

The EHL slip model provides quantitative predictions of the characteristic velocity V^* and sliding yield stress σ_s, which can be compared to the experimental values.[35] The expression of the characteristic velocity V^* involves both particle and suspension properties according to:

$$V^* \text{ ffi } 0{:}4\gamma_y^2 \left(\frac{G_0 R}{Z_s}\right)\left(\frac{G_P}{G_0}\right)^{1/3} \quad (2)$$

where G_0 is the suspension storage modulus, Z_s is the solvent viscosity, γ_y is the yield strain and R is the particle radius. The parameter G_P^* is the effective contact modulus which is a function of the shear modulus and the Poisson ratio of the particles, respectively G_P and ν: $G_P^* = 2pG_p/(1 - \nu)$. We have computed the values of the characteristic velocity V^* which are expected from this expression using the values of γ_y, G_0 and G_p, reported in Tables 1 and 2, and taking R = 1.1 mm, Z_s = 1 mPa s and ν = 0.35. In Table 3, we observe a good agreement between the predictions of the EHL slip model and the experimental values.

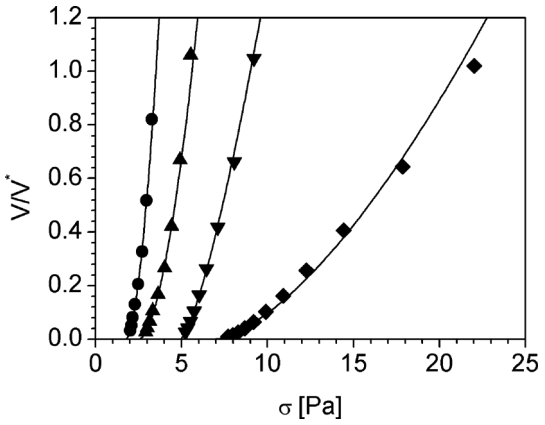

Fig. 4 Variations of the reduced slip velocity V/V^* against the applied shear stress. The symbols represent the values deduced from the apparent flow curves in the regime of total slip below the yield stress. The continuous lines are the best fits of the experimental data to eqn (1).

4.4 Scaling the slip yield stress

The slip yield stress represents the minimum stress below which no apparent motion can be detected. In this regime where $\sigma < \sigma_s < \sigma_y$, yield stress materials behave essentially like weak elastic solids that undergo plastic rearrangements without ever reaching steady state.[60–62] The existence of the slip yield stress has been related to the existence of short range forces between the particles and the wall. When the net interaction is repulsive, the shearing surfaces are covered by a continuous lubricating film of solvent and $\sigma_s = 0$. For attractive interactions, particles can stick to surfaces and σ_s is finite.[28,29,36,37] Seth *et al.* estimated the slip yield stress as the stress value where the repulsive lift force induced by EHL becomes larger than the attractive particle–wall interactions.[36] For particle–surface interactions dominated by dispersion forces, σ_s was been predicted to vary as: $\sigma_s = G_0^{3/4} A^{1/4} / R^{3/4}$, where G_0 is the plateau shear modulus of the suspension, A is the effective Hamaker constant which accounts for the attractive van der Waals interactions between the agarose microparticles and the silicon surface; R is the radius of the microparticles. The variations of the slip yield stress with the plateau modulus for the five concentrations under investigation are shown in Fig. 5. They are compared to similar data for polyelectrolyte microgels reprinted from Seth *et al.*[36] Remarkably, the two sets of data follow similar variations which are well described by power laws with exponents of the order of 0.67. These power laws are fully compatible with the theoretical prediction. We note that the two sets of data are shifted vertically in logarithmic scale. Agarose particles (R = 1.1 mm) being larger than polyelectrolyte microgels (R = 0.3 mm), the data for agarose particles should lie slightly below the data for polyelectrolyte microgels. However, we observe the opposite. For the difference in Hamaker constants to compensate for the differences in radii (factor 2.5) and explain the vertical shift in Fig. 5 (factor 3), the Hamaker constants should be in the ratio 3000. Hamaker constants are not known precisely but we can make a rough comparison based on particle densities. If we consider that the volume fraction of polymer in the polyelectrolyte microgels is about 0.01 while in agarose particles it is about 1, this would result in a ratio of 100 between the two particle types, which is not sufficient to explain the discrepancy observed in Fig. 5.

The inset compares the variations of the slip yield stress scaled with the particle modulus G_p *versus* the bulk modulus G_0. We observe that the two sets of data collapse. It is not clear from the theoretical prediction above why σ_s/G_p should scale with G_0 and why the data for polyelectrolyte microgels and agarose particles collapse. Albeit, the above analysis has defined σ_s to be a function of the forces perpendicular to the plate only, our result suggests that the contributions from the friction in the shearing plane cannot be excluded, allowing for σ_s to be influenced by the particle modulus. Soft tribology studies involving sliding/rolling ball-on-disk show that the limits of lubrication and friction are dependent on the mechanical properties of the substrates. In particular, at low entrainment speeds, friction is not only

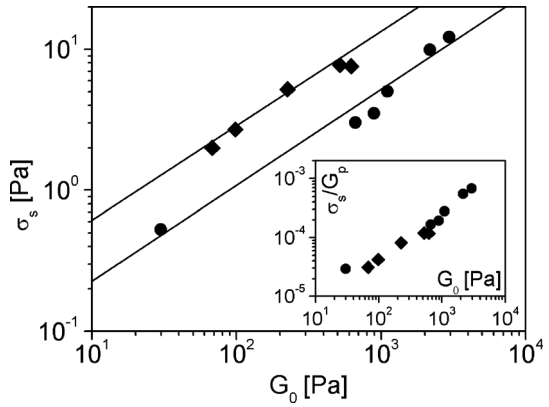

Fig. 5 Variations of the slip yield stress (σ_{ss}) with the suspension storage modulus (G_0) for agarose particles on a silicon surface (■) and polyelectrolyte microgels on gold and Scotch® tape surfaces (●) replotted from Seth *et al.*[36] Continuous lines are power law fits to the experimental data (exponent of 0.67). The inset shows the collapse of the two sets of experimental data when the sliding yield stress is scaled by the particle modulus.

dependent on adhesive forces but also on a rolling-friction contribution that is a function of the hysteresis losses in viscoelastic substrates, namely the product of loss tangent ($\tan\delta = G''/G'$) and the ratio of Hertzian contact area and ball radius.[63,64] Since $\tan\delta$ is anticipated to be substantially lower for agarose particles than for polyelectrolyte microgels, friction forces are predicted to be significantly greater, which coincides with the observation that σ_{ss} is greater for the more viscoelastic agarose particles. To confirm this hypothesis, further investigation is required using Atomic Force Microscopy for instance, to evaluate the interplay between friction and adhesive forces for both particle types.

5. Concluding remarks

The phenomenon of slip during flow of dense suspensions of non-Brownian hydrogel microparticles has been analyzed in terms of the tribology interactions occurring between the particles and the shearing surface. The elastohydrodynamic slip model provides quantitative predictions of the variations of the slip velocity with the stress, of the characteristic velocity at the shearing surfaces and of the slip yield stress. The latter is the shear stress corresponding to the onset of sliding of the suspensions confined between smooth surfaces, which is smaller than the bulk suspension yield stress. We have extended the conventional steady shear investigations of slip to unsteady solicitations like LAOS. During LAOS, there is a reversible transition between adhesion at the surface, slip and elastic deformation as the shear stress is varied. Both situations share the same generic features, the bulk yield stress and the slip yield stress playing similar roles albeit reflecting bulk and interfacial yielding respectively. One pending question concerns the origin of the slip yield stress. We found that it is a function of both the adhesive attractive forces between the particle and wall but our results also suggest that it depends on the particle viscoelasticity though the friction associated with hysteresis losses within the particles. This result needs further elaboration and calls for future tribology experiments.

Acknowledgements

We would like to acknowledge Dr Gleb Yakubov (University of Queensland) for helpful discussions. HMS gratefully acknowledges financial support from an Australian Postgraduate Award Scholarship and The University of Queensland Graduate School International Travel Award. HMS thanks Ludwik Leibler for his support for the work at ESPCI Paris in the Soft Matter and Chemistry Laboratory, also Charlotte Pellet for her help in the laboratory. JRS acknowledges support from Australian Research Council Discovery Project DP150104147.

References

1 H. A. Barnes, *J. Non-Newtonian Fluid Mech.*, 1995, 56, 221.
2 M. Cloitre and R. T. Bonnecaze, *Rheol. Acta*, 2016, under review.
3 A. Yoshimura and R. K. Prud'homme, *J. Rheol.*, 1988, 32, 53.
4 J. Chen and J. R. Stokes, *Trends Food Sci. Technol.*, 2012, 25, 4.
5 D. A. Fedosov, H. Noguchi and G. Gompper, *Biomech. Model. Mechanobiol.*, 2014, 13, 239.
6 R. H. Ewoldt, C. Clasen, A. E. Hosoi and G. H. McKinley, *Soft Matter*, 2007, 3, 634.
7 K. Wolff, D. Marenduzzo and M. E. Cates, *J. R. Soc., Interface*, 2012, 9, 1398.
8 D. D. Joseph, *Powder Technol.*, 1997, 97, 211.
9 R. Mezzenga, P. Schurtenberger, A. Burbidge and M. Michel, *Nat. Mater.*, 2005, 4, 729.
10 J. R. Stokes and W. J. Frith, *Soft Matter*, 2008, 4, 1133.
11 J. J. Stickel and R. L. Powell, *Annu. Rev. Fluid Mech.*, 2005, 37, 129.
12 A. Lawal and D. M. Kalyon, *Numer. Heat Transfer, Part A*, 1994, 26, 103.
13 D. M. Kalyon, A. Lawal, R. Yazici, P. Yaras and S. Railkar, *Polym. Eng. Sci.*, 1999, 39, 1139.
14 D. M. Kalyon, *Polym. Eng. Sci.*, 2010, 50, 652.
15 E. Birinci and D. M. Kalyon, *J. Rheol.*, 2006, 50, 313.
16 H. S. Tang and D. M. Kalyon, *J. Rheol.*, 2008, 52, 1069.
17 L.-H. Luu and Y. Forterre, *J. Fluid Mech.*, 2009, 327, 632.
18 A. Saïdi, C. Martin and A. Magnin, *Exp. Fluids*, 2011, 51, 211.
19 Y. Damianou, M. Philippou, G. Kaoullas and G. C. Georgiou, *J. Non-Newtonian Fluid Mech.*, 2014, 203, 24.
20 M. Philippou, Z. Kountouriotis and G. C. Georgiou, *J. Non-Newtonian Fluid Mech.*, 2016, 234, 69.
21 M. Mooney, *J. Rheol.*, 1931, 2, 210.
22 U. Yilmazer and D. M. Kalyon, *J. Rheol.*, 1989, 33, 11197.
23 D. M. Kalyon, *J. Rheol.*, 2005, 49, 621.
24 M. Habibi, M. Dinkgreve, J. Paredes, M. M. Denn and D. Bonn, *J. Non-Newtonian Fluid Mech.*, 2016, 238, 33.
25 G. A. Davies and J. R. Stokes, *J. Non-Newtonian Fluid Mech.*, 2008, 148, 73.
26 E. C. Bingham, *Fluidity and plasticity*, McGraw-Hill, New York, 1922.

27 R. Buscall, *J. Rheol.*, 2010, 54, 1177.
28 P. Ballesta, G. Petekidis, I. Isa, W. C. K. Poon and R. Besseling, *Phys. Rev. Lett.*, 2008, 101, 258201.
29 P. Ballesta, G. Petekidis, L. Isa, W. C. K. Poon and R. Besseling, *J. Rheol.*, 2012, 56, 1005.
30 S. Ghosh, D. van den Ende, F. Mugele and M. H. G. Duits, *Colloids Surf.*, 2016, A491, 50.
31 S. C. Jana, B. Kapoor and A. Acrivos, *J. Rheol.*, 1995, 39, 1123.
32 M. Korhonen, M. Mohtaschemi, A. Puisto, X. Illa and M. J. Alava, *Eur. Phys. J. E: Soft Matter Biol. Phys.*, 2015, 38, 46.
33 V. Bertola, F. Bertrand, H. Tabuteau, D. Bonn and P. Coussot, *J. Rheol.*, 2003, 47, 1211.
34 S. P. Meeker, R. T. Bonnecaze and M. Cloitre, *Phys. Rev. Lett.*, 2004, 92, 198302.
35 S. P. Meeker, R. T. Bonnecaze and M. Cloitre, *J. Rheol.*, 2004, 48, 1295.
36 J. R. Seth, M. Cloitre and R. T. Bonnecaze, *J. Rheol.*, 2008, 52, 1241.
37 J. R. Seth, C. Locatelli-Champagne, F. Monti, R. T. Bonnecaze and M. Cloitre, *Soft Matter*, 2012, 8, 140.
38 T. Divoux, V. Lapeyre, V. Ravaine and S. Manneville, *Phys. Rev. E: Stat., Nonlinear, Soft Matter Phys.*, 2015, 92, 060301.
39 A.-L. Vayssade, C. E. Terriac, F. Monti, M. Cloitre and P. Tabeling, *Phys. Rev. E: Stat., Nonlinear, Soft Matter Phys.*, 2014, 89, 052309.
40 S. Aktas, D. M. Kalyon, B. M. Marín-Santibáñez and J. Pérez-González, *J. Rheol.*, 2014, 58, 513.
41 B. D. Jofore, P. Erni, G. Vleminckx, P. Moldenaers and C. Clasen, *Rheol. Acta*, 2015, 54, 581.
42 J. B. Ortega-Avila, J. Pérez-González, B. M. Marín-Santibáñez, F. Rodríguez-González, S. Aktas, M. Malik and D. M. Kalyon, *J. Rheol.*, 2016, 60, 503.
43 H. J. Walls, S. B. Caines, A. Sanchez and J. Khan, *J. Rheol.*, 2012, 47, 847.
44 W. J. Frith and A. Lips, *Adv. Colloid Interface Sci.*, 1995, 6, 161.
45 W. J. Frith, A. Lips and I. T. Norton, *Structure and Dynamics of Materials in the Mesoscopic Domain*, World Scientific, 1999.
46 S. Adams, W. J. Frith and J. R. Stokes, *J. Rheol.*, 2004, 48, 1195.
47 P. Burey, B. R. Bhandari, T. Howes and M. J. Gidley, *Crit. Rev. Food Sci. Nutr.*, 2008, 48, 361.
48 H. M. Shewan and J. R. Stokes, *J. Food Eng.*, 2013, 119, 781.
49 R. Borrega, M. Cloitre, I. Betremieux, B. Ernst and L. Leibler, *Europhys. Lett.*, 1999, 47, 729.
50 H. M. Shewan and J. R. Stokes, *J. Colloid Interface Sci.*, 2015, 442, 75.
51 C. Pellet and M. Cloitre, *Soft Matter*, 2016, 12, 3710.
52 R. S. Farr and R. D. Groot, *J. Chem. Phys.*, 2009, 131, 244104.
53 H. M. Shewan and J. R. Stokes, *J. Non-Newtonian Fluid Mech.*, 2015, 222, 72.
54 L. Mohan, C. Pellet, M. Cloitre and R. Bonnecaze, *J. Rheol.*, 2013, 57, 1023.
55 B. M. Erwin, M. Cloitre, M. Gauthier and D. Vlassopoulos, *Soft Matter*, 2010, 6, 2825.
56 T. G. Mason, J. Bibette and D. A. Weitz, *J. Colloid Interface Sci.*, 1996, 179, 439.
57 D. Vlassopoulos and M. Cloitre, *Curr. Opin. Colloid Interface Sci.*, 2014, 19, 561.
58 J. R. Seth, L. Mohan, C. Locatelli-Champagne, M. Cloitre and R. T. Bonnecaze, *Nat. Mater.*, 2011, 10, 838.
59 H. Shewan, *Rheology of soft particle suspensions*, PhD thesis, The University of Queensland, 2015, DOI: 10.14264/uql.2015.533.
60 S. M. Fielding, P. Sollich and M. E. Cates, *J. Rheol.*, 2000, 44, 323.
61 M. Cloitre, R. Borrega and L. Leibler, *Phys. Rev. Lett.*, 2000, 85, 4819.
62 L. Cipelletti, L. Ramos, S. Manley, E. Pitard, D. A. Weitz, E. E. Pashkovski and M. Johansson, *Faraday Discuss.*, 2003, 123, 237.
63 C. Myant, H. A. Spikes and J. R. Stokes, *Tribol. Int.*, 2010, 43, 55.
64 J. A. Greenwood and D. Tabor, *Proc. Phys. Soc., London*, 1958, 71, 989.

